Published in final edited form as:
J Am Chem Soc. 2011 August 10; 133(31): 12247–12255. doi:10.1021/ja204578e.

Light-induced Release of DNA from Gold Nanoparticles: Nanoshells and Nanorods

Ryan Huschka[†], **Jorge Zuloaga**[‖], **Mark Knight**[§,‡], **Lisa V. Brown**[†], **Peter Nordlander**[§,‡,⊥,‖], and **Naomi J. Halas**[*,§,†,‡,⊥,‖]

[†]Department of Chemistry, Rice University, Houston, TX 77005

[§]Department of Electrical and Computer Engineering, Rice University, Houston, TX 77005

[‖]Department of Physics and Astronomy, Rice University, Houston, TX 77005

[‡]Laboratory for Nanophotonics, Rice University, Houston, TX 77005

[⊥]Department of Bioengineering, Rice University, Houston, TX 77005

Abstract

Plasmon-resonant nanoparticle complexes show highly promising potential for light-triggered, remote-controlled delivery of oligonucleotides on demand, for research and therapeutic purposes. Here we investigate the light-triggered release of DNA from two types of nanoparticle substrates: Au nanoshells and Au nanorods. Both light-triggered and thermally induced release are distinctly observable from nanoshell-based complexes, with light-triggered release occurring at an ambient solution temperature well below the DNA melting temperature. Surprisingly, no analogous measureable release was observable from nanorod-based complexes below the DNA melting temperature. These results suggest that a nonthermal mechanism may play a role in plasmon resonant, light-triggered DNA release.

Keywords

Plasmon; nanoshell; nanorod; hot electron; photoinduced electron transfer; enhanced local field; photothermal; DNA

Introduction

For many reasons, Au nanoparticle-based complexes show great promise for a wide variety of biomedical applications. Their small size relative to eukaryotic cell dimensions facilitates intracellular uptake (endocytosis), providing an effective method for the transfection of adsorbate "cargo" molecules into the intracellular environment. Au nanoparticle surfaces can be readily functionalized with thiolated molecules, taking advantage of the strong Au-S

[*]Corresponding author, halas@rice.edu..

Supporting Information Available: Data for additional experiments: stability of fluorophore under laser excitation, Au-thiol bond stability, ssDNA release of adsorbed DNA, release curve dependent upon nanoshell concentration, and raw data showing release of ssDNA from nanorods with 120 dsDNA per nanorod. This information is available free of charge via the Internet at http://pubs.acs.org/.

bond, enabling the formation of functional nanocomplexes. This "Au nanoparticle + molecular layer" platform provides a general functional strategy for designing nanocomplexes with specific, and often multiple, functionalities. Examples of functional or multifunctional nanocomplexes constructed in this manner include enhanced fluorescence and MRI contrast agents for bioimaging, delivery vectors for molecular chemotherapeutics or oligonucleotides for gene therapy. [1-4]

Au-based nanoparticles of various morphologies offer additional functionality because of their optical properties, derived from the characteristics of their localized surface plasmon. Examples of Au-based nanoparticles of interest for biomedical applications include nanoshells, nanorods, nanocages, and other geometries,[5-12] that allow the plasmon resonance to be shifted from the visible into the physiological "water window" in the near infrared region of the spectrum.[13] Illumination at their plasmon resonant frequency results in light absorption, where the absorbed energy is efficiently converted to heat and can be exploited for hyperthermal cancer therapy[14,15] or photothermal drug delivery.[4,16-18] Plasmonic nanoparticles larger than the dipole (i.e., quasistatic) limit are also highly effective light scatterers, a property advantageous for bioimaging.[19] Additionally, plasmonic nanoparticles can modify the optical density of states of nearly adjacent fluorophores, decreasing their radiative lifetime and increasing their quantum yield, enhancing their fluorescence.[20-24] This property is particularly advantageous for bioimaging, since it can be used to improve the quantum yield of fluorophores already in widespread use, enhancing popular imaging modalities such as optical tomography.[25,26] An additional property of the plasmon resonance of nanoparticles, frequently overlooked, is the generation of nonequilibrium "hot" electron-hole pairs, a dominant mechanism for plasmon decay.[27] In addition to damping the plasmon resonance,[28] hot electrons can react with molecules at the surface of the metal nanoparticle, resulting in enhanced photoinduced charge transfer reactions.[29-31]

The light-triggered, remotely controlled release of oligonucleotides from plasmonic nanoparticle-based complexes is an important application that has recently begun to be investigated. Thus far, light-induced release has been demonstrated using two general strategies. One approach consists of attaching the cargo molecules to be delivered directly to the nanoparticle surface, typically through a Au-thiol bond, then using femtosecond laser pulses to reshape the nanoparticles and break the Au-S bond.[17,18,32,33] This approach presents significant risk for *in vivo* applications: the incident energy sufficient to reshape plasmonic nanoparticles may very well be sufficient to induce cell death, and the smaller sized nanoparticles resulting from this process have been shown to have toxic effects. [34,35] In the second method, a "host" molecule is first attached to the nanoparticle surface, typically via a Au-thiol bond, then the cargo molecule is complexed, not to the nanoparticle surface, but to the host molecule via weaker, noncovalent interactions. When this type of nanocomplex is illuminated with light at a wavelength corresponding to the plasmon resonance of the dressed nanoparticle,[4,36-38] the attraction between host and cargo species is reduced and the therapeutic molecules are released. This release strategy shows excellent promise for light-controlled delivery due to the relatively low laser power densities and short irradiation times required to achieve release of molecular cargo.

Recently we demonstrated light-induced release of single-stranded deoxyribonucleic acid (ssDNA) from plasmonically tunable Au nanoshells, nanoparticles consisting of a spherical silica (SiO_2) core surrounded by a Au shell.[39] Nanoshells with their plasmon resonance wavelength at 800 nm were coated with double-stranded DNA (dsDNA), where one strand of the DNA possessed a terminal thiol moiety on its 5' end for attachment to the nanoshell surface. In this configuration, one strand of the DNA serves as the host molecule. The complementary DNA cargo sequence hybridized to the host molecule was nonthiolated, and therefore, when hybridized, was bound only to its DNA complement host and not the nanoparticle surface. Upon 800 nm laser illumination, the dsDNA was dehybridized, releasing the nonthiolated ssDNA sequence. The properties of light-induced DNA release performed in this manner were compared to that of thermally induced DNA release, where the nanocomplex solution was immersed in a thermal bath and the amount of DNA released as a function of solution ambient temperature was observed.[39] Several striking differences between light-induced release and thermally induced release of ssDNA from this nanocomplex can be observed. For the light-induced case, DNA release occurs with minimal increase in solution ambient temperature, and appears largely independent of oligonucleotide length in the 20-70 base pair range. Thermally-induced release occurs at the DNA melting temperature, which is dependent upon oligonucleotide and composition, attachment to the nanoparticle surface, and properties of the solution, such as ion and nanoparticle concentration. Another marked difference between light-induced and thermally-induced release is the efficiency of DNA release. In the light-induced case, only a fraction of the ssDNA loaded onto the nanocomplexes is released, whereas for thermal release, virtually all the ssDNA cargo is released when the solution ambient temperature is increased above the DNA melting temperature. These contrasting properties prompt questions regarding the light-induced ssDNA release process, and motivate the current study.

Here we directly compare the light-induced and thermally-induced release of ssDNA from two different types of plasmonic nanoparticles: Au nanoshells and Au nanorods. Both types of nanoparticles were designed and synthesized with spectrally overlapping plasmon resonances. The release of ssDNA from both types of nanocomplexes was quantified for both light-triggered and thermally induced ssDNA release. For light-induced ssDNA release from nanoshells, both light-induced and thermally induced contributions to ssDNA release are distinctly observable as the solution ambient temperature increases due to laser heating. This release profile allows us to discriminate clearly between the light-induced and thermally induced contributions to ssDNA release in the light-induced case. For nanorod-based complexes, both light-induced and thermally induced ssDNA release show virtually the same thermal profile, with a clear threshold for DNA release occurring at the DNA melting temperature in all cases. This contrast between nanoshell-based and nanorod-based light-induced ssDNA release can be interpreted in terms of an additional, nonthermal contribution that assists ssDNA dehybridization in the light-induced case. In our experiments, this contribution appears to be more efficient for nanoshell-based complexes than for the nanorod-based complexes investigated.

Results

Synthesis and Characterization of Au Nanoshells and Au Nanorods

Both Au nanorods and Au nanoshells are prime examples of nanoparticles whose properties are geometrically tunable across a range of wavelengths in the visible and near-infrared regions of the spectrum. Nanorods have two primary plasmonic modes, whose excitation is sensitive to the polarization of incident light: the transverse mode, where the collective electronic oscillation of the plasmon occurs perpendicular to the major axis of the nanoparticle, and the longitudinal mode, where the plasmon oscillation occurs parallel to the major axis of the nanoparticle. While the resonance wavelength of the Au nanorod transverse plasmon is similar to that for Au colloid (~520 nm), the longitudinal resonance wavelength increases with increasing aspect ratio.[40] Similarly, for nanoshells, the wavelength of the plasmon resonance can be tuned from the visible into the near-infrared by varying the thickness of the Au shell relative to the size of the silica (SiO_2) core.[41]

The nanoparticles used in this series of experiments are shown schematically in Figure 1A. Silica core/Au shell nanoshells were synthesized using previously published methods.[42] A scanning electron microscope (SEM) image of [r_1, r_2] = [60, 76] nm nanoshells is shown in Figure 1B. The core and shell radii were obtained from particle size statistics obtained from SEM images of over 100 silica core particles and 100 Au-coated nanoshells. Au nanorods were synthesized according to the seed-mediated growth method using Cetyltrimethylammonium Bromide (CTAB) as a surfactant.[43] This method results in nanorods with high yields and a low polydispersity, to ensure uniform nanoparticle-to-nanoparticle plasmon resonance wavelengths. A representative transmission electron microscopy (TEM) image of [w, l] = [13, 47] nm nanorods is shown in Figure 1C. These length and width measurements are from particle size statistics of over 100 nanorods from TEM images. The extinction spectra of the nanoshells and nanorods synthesized for these experiments are shown in Figure 1D. The extinction maximum of nanoshells was observed at 797nm, and that of nanorods was observed at 788 nm, well within the broader spectral envelope of the nanoshell plasmon resonance. For all experiments, the optical density of the samples were adjusted to be equivalent at the laser wavelength of 800 nm For the nanoparticles used, the extinction cross section of a nanorod is nearly an order of magnitude smaller than that of a nanoshell, therefore maintaining a constant optical density required a higher nanorod concentration relative to nanoshells. To adjust the optical density of the two solutions to be roughly equivalent for both samples, we used a concentration of 30 pM for nanoshells and 1 nM for nanorods. Keeping the optical density equivalent for both samples allows quantitative comparisons of light-triggered release for both nanoparticle morphologies.

Attachment of DNA to Au nanoshells and Au nanorods

Both types of nanoparticles were functionalized with DNA oligonucleotides. In both cases, the cargo sequence is tagged with a fluorescein molecule in order to quantify nanoparticle surface coverages and ssDNA release. The host and cargo DNA were hybridized, then bound to the nanoparticle surfaces via the thiol modification on the host DNA. The nanoshells were incubated with hybridized dsDNA as previously reported.[39] Hybridized

dsDNA was attached to the nanorods by using a roundtrip phase transfer ligand exchange method[44] (See Methods section). Nanorods require a different functionalization protocol because of the need to displace residual CTAB molecules remaining on the as-synthesized nanorods following growth. This method allows dsDNA functionalization of nanorods without any harsh sonication or heating steps that other functionalization methods require. For both nanoshells and nanorods, the same 20-base dsDNA sequence is used (see Methods section).

To confirm dsDNA attachment to both the nanoshells and nanorods, mercaptoethanol was used to displace the dsDNA.[45] After displacement, the sample was centrifuged to separate the displaced DNA from the nanoparticles, a necessary step to isolate the fluorescently-tagged DNA from the gold nanoparticles, since fluorescence quenching or enhancement may occur. The fluorescence of the supernatant was measured, and the amount of DNA displaced was quantified. Dividing by the nanoparticle concentration, obtained from UV-Vis extinction measurements, yields the number of DNA molecules released per nanoparticle. For nanorods, the surface coverage is ~40 dsDNA per nanorod (normalized by surface area is ~ 4.4 pmol/cm^2); for nanoshells the coverage is approximately ~5000 dsDNA per nanoshell (~11.5 pmol/cm^2). The lower surface coverage observed for nanorods is a result of a much smaller surface area per nanoparticle (the nanorod surface area is nominally 33 times smaller than the nanoshell surface area), and is also due to the difficulty of functionalizing nanorods caused by the bilayer of CTAB surfactant surrounding the gold nanorod in solution, which limits coverage for dsDNA functionalization. Although CTAB-free synthesis methods exist, they typically have a significantly higher degree of polydispersity and therefore significant inhomogeneous broadening of the spectral lineshape, and were therefore not pursued for this series of experiments.

Light-induced and thermal release of cargo DNA from Au Nanoshells

Thermal treatment consists of placing a 3 mL solution of the nanoshell-dsDNA sample in a centrifuge tube, placing the centrifuge tube in a water bath and heating the water bath slowly (~1°C/minute) while stirring. The slow heating and stirring ensures that the nanoshell-dsDNA sample is in thermal equilibrium during the entire course of the measurement. Laser treatment consists of placing a 3mL solution of the nanoshell-dsDNA sample in a centrifuge tube, then irradiating the sample with a continuous wave NIR laser (λ_{LASER} = 800 nm, 1.3 W/cm^2) at the peak plasmon resonance of the nanoshell while stirring the sample. Due to the photothermal properties of nanoshells, this laser excitation also results in bulk heating of the solution. In both thermal and laser treatments, the solution temperature is monitored by a thermocouple. The dehybridization and release of the fluorescein-tagged ssDNA is monitored by removing aliquots from the solution as the solution temperature rises. Each aliquot is centrifuged to separate the released DNA from the nanoparticles, and the fluorescence intensity of the supernatant is monitored to determine the number of ssDNA molecules released per nanoparticle.

A schematic of the release of DNA from gold nanoshells is shown in Figure 2A, where the host DNA sequence is shown in red, and the cargo DNA sequence is depicted in blue. A comparison of light-induced and thermally induced DNA release from nanoshells is shown

in Figure 2B. The thermally induced release (Figure 2B, black squares) is characteristic of DNA melting, with a sharp onset at the effective DNA melting temperature. The melting temperature of DNA is determined as half the increase in released DNA, which, for the nanocomplexes shown here, occurs at 60° C. By comparison, light-induced DNA release (Figure 2B, red circles) results in a quite different DNA release curve. A significant fraction of the DNA is released at solution temperatures well below the DNA melting temperature. Approximately 20% of the DNA was observed to be released below the melting temperature threshold. The inset shows an expanded view of the temperature range below that of the DNA melting temperature range. For ambient solution temperatures above 50°C, DNA release is extremely similar for both heating mechanisms.

The percentage of DNA released under illumination appears highly reproducible within each prepared batch, yet varies at the batch-to-batch level in the nominal range of 20-50% over a range of experimental factors, depending upon nanoshell concentration, illumination geometry, and adsorbate concentration and structure.[39,46] We also observe that the thermally induced release, which results in nearly 100% DNA release, shows batch-to-batch variations in the DNA melting temperature that vary based on nanoparticle and adsorbate concentration. To ensure that the Au-thiol bond was not broken in these experiments, a control experiment was performed in which a fluorescently tagged thiolated single-stranded DNA sequence was attached to gold nanoshells. Under identical thermal and laser treatment conditions, the release of this thiolated ssDNA was not observed, which demonstrated the Au-thiol bond is not broken as a result of either the thermal or laser treatments. (Supporting Information, Figure S2).

The amount of time required for the entire heating process in the laser treatment is approximately 12 minutes (top axis, Figure 2B), however, the light-induced release begins immediately, making this method suitable for controlled delivery of therapeutic molecules. The time scale is not linear: at higher temperatures, more time is required to heat the solution, due continuous heat loss by the experimental container to the surroundings during the course of the experiment.

Light-induced and thermal release of cargo DNA from Au Nanorods

The light-induced release of DNA from nanorods (Figure 3A) was investigated with an identical protocol to that used for nanoshells. For each nanorod-dsDNA sample we compared the thermal treatment DNA release curve to the laser treatment DNA release curve with all of the experimental conditions for the nanorod-dsDNA samples identical to the nanoshell-dsDNA experiments (see methods section). Additionally, we investigated the light-induced release of DNA from nanorods by exciting the transverse plasmon resonance of the nanorod with a 532 nm CW laser. For nanorods, we fully expected to see a similar trend in the light-induced process with respect to our observations for nanoshells, but to our surprise, the nanorods did not exhibit light-induced release of DNA.

The thermal treatment of the nanorod-dsDNA sample results in a ssDNA release curve with a melting temperature of ~ 45°C (Figure 3B, black squares). NIR laser irradiation (λ_{LASER} = 800 nm, 1.3 W/cm^2), which drives the longitudinal plasmon resonance of the nanorod results in a ssDNA release curve (Figure 3B, red dots) that looks extremely similar to the

thermal ssDNA release curve, with no measureable increase in DNA release at temperatures significantly below the thermal temperature. The inset highlights the temperature range, 40°C and below, prior to thermal melting where light-induced release would be clearly distinguishable if it were observed. The entire heating process for the longitudinal laser treatment on the nanorod-DNA sample takes about 6 minutes (Figure 3B, top axis) which is approximately half the time of the nanoshell sample. This faster heating in the nanorod solution occurs because the nanorods absorb a higher percentage of light than they scatter due to their smaller size. The optical density (total extinction cross section) of both the nanoshell-DNA and nanorod-DNA samples were kept constant, so the nanorod solution absorbs a higher percentage of the light resulting in faster heating of the sample. The lack of light-induced release below the DNA melting temperature is therefore surprising if the process is driven by a nonequilibrium thermal mechanism: however, the thermal response observed here is consistent with another recent study of this system.[47]

Next, we investigated light-induced release of DNA from nanorods when the transverse plasmon resonance is excited. The thermal treatment for this nanorod-DNA sample (Figure 3C, black squares) results in a dsDNA melting temperature of ~ 50°C. The laser treatment (λ_{LASER} = 532nm, 25 W/cm^2) exciting the transverse plasmon results in a DNA release curve that again looks similar to the thermal treatment (Figure 3C, green dots). The inset highlights the temperature range, 45°C and below, prior to thermal DNA release where light-induced release would be distinguishable, if it were observed. The heating with the 532 nm laser for the transverse excitation of nanorods occurs the fastest (3.5 minutes), but light-induced release was still not observed. The faster heating occurs for several reasons. At this excitation wavelength, direct absorption of light by water is significantly greater than at 800 nm; additionally, the intensity of the incident laser was increased from 1.3 to 25 W/cm^2 to compensate for the smaller absorption cross section of the transverse plasmon resonance. Also, for randomly oriented nanorods in solution under polarized light excitation, twice as many will be excited with transverse polarization relative to longitudinal polarization since there are twice as many orientations where the transverse plasmon would be excited.[48] If we compare the nanoshell and the nanorod heating experiments during the time window prior to DNA melting: for nanoshells there was significant DNA release, while for nanorods there was virtually no DNA release.

Discussion

As is clearly observed, the laser-induced DNA release that is observed on nanoshell substrates occurs at a significantly lower solution temperature than DNA melting on the same nanoparticle substrate, indicating that dehybridization of DNA occurs faster than macroscopic heating of the solution. There are two plausible mechanisms that may account for this behavior: a nonequilibrium thermal mechanism, or a nonthermal mechanism. In a nonequilibrium thermal process, the irradiated nanoparticle would undergo a very rapid local temperature increase at its surface, providing enough local heating to melt the DNA molecules prior to increasing the ambient solution temperature. A nonthermal mechanism would involve a process related to the excitation of the nanoparticle surface plasmon, such as the transfer of hot electrons from the metal to the adsorbate DNA,[27,49] which would increase the electrostatic repulsion between DNA strands resulting in DNA dehybridization.

Following excitation, the nanoparticle plasmon can decay either by radiative damping (scattering) or energetic relaxation (absorption via Landau damping), which creates nonequilibrium electron-hole pairs.[50] These "hot" excited electrons undergo rapid electron-electron scattering and within a few femtoseconds establish a nonequilibrium hot electron distribution that can be characterized by an elevated temperature. This hot electron distribution then thermalizes with the lattice via electron-phonon coupling on a picosecond timescale. This energy is then dissipated to the surrounding medium via phonon-phonon coupling within hundreds of picoseconds, which results in heating of the ambient solution.[28] When molecules are adsorbed on the metallic nanoparticle surface, excited "hot" electrons can transfer to the adsorbate prior to thermalization.[30,31,50] Numerous groups have observed photoinduced charge transfer under low intensity CW laser illumination conditions at the peak plasmon resonance of metal nanoparticles.[30,49,51]

Nonequilibrium Thermal Mechanism

To understand our observations of DNA release relative to the energy dissipation and heating occurring in our nanoparticle solutions we need to understand these processes in greater detail. In all experiments reported, the interparticle distances are sufficient to eliminate interparticle coupling between the plasmon-enhanced electric fields, which can affect the local heat generated around a nanoparticle. For the nanoshelldsDNA and nanorod-dsDNA solutions, the particle density is 1.8×10^{10} nanoshells/mL and 6.14×10^{11} nanorods/mL, which gives an interparticle spacing of 3.8 μm and 1.2 μm, respectively. Each individual nanoparticle can be considered as an independent heat source, and plasmon coupling can be neglected. The localized increase in temperature around a single nanoparticle depends upon the absorption cross section, laser intensity, size of the nanoparticle, and thermal conductivities of both the metal and surrounding medium. [52-56] The temperature increase on the surface of an individual nanoparticle in aqueous solution is:[52]

$$\Delta T_{NP} = \frac{\sigma_{abs} \mathrm{I}}{4\pi \mathrm{R}_{eq} \beta \kappa_{\mathrm{water}}} \quad (1)$$

where σ_{abs} = absorption cross section (m^2), I = intensity of the incident light (W/m^2), R_{eq} = radius of a sphere with the same volume as the particle ($R_{eq} = (3V_{NP} / 4\pi)^{1/3}$ m), β = Thermal capacitance coefficient dependent on nanoparticle aspect ratio (AR) ($\beta = 1 + 0.96587(\ln^2(\mathrm{AR}))$) and κ_{water} = thermal conductivity of water. For the thermal capacitance coefficient, the aspect ratio of the nanoshell and nanorod is 1 and 3.6, respectively. For our series of experiments, the absorption cross sections for nanoshells and nanorods used were $\sigma_{abs,NS} = 1\times10^{-14}$ m^2, $\sigma_{abs,NR} = 2.75\times10^{-15}$ m^2, [48] I = 1.3 W/cm^2, $R_{eq,NS}$ = 75nm, $R_{eq,NR}$ = 11.6nm, $\beta_{NS} = 1$, $\beta_{NR} = 2.65173$, and κ_{water} = 0.6W/mK. Based on these parameters, we calculate theoretical temperature increases of $\Delta T_{NS} = 2.3\times10^{-4}$ K and $\Delta T_{NR} = 1.5\times10^{-4}$ K at the nanoshell and nanorod surfaces, respectively. These small increases in temperature on the surface of the nanoparticles are primarily a result of the low CW optical intensities used in these experiments (1.3 W/cm^2). To obtain a significant temperature increase on the nanoparticle surface, optical intensities would be required to be ~10^4-10^5 W/cm^2, requiring

pulsed laser sources.[53] The observed ambient solution heating must therefore be a result of accumulative heating, in agreement with similar analyses by Govorov and coworkers.[54-56]

Nonthermal Mechanism

The very small increases in nanoparticle surface temperature estimated for our experimental conditions suggest that a nonthermal mechanism may be responsible for light-triggered release. Since the creation of nonequilibrium hot electrons is a direct result of plasmon excitation of the nanoparticle, the greatest number of hot electrons will be generated by illumination at the plasmon resonance of the nanoparticle, where absorption is the highest. The probability of charge transfer increases with an increasing number of hot electrons. Because hot electron generation is dependent upon absorption, the magnitude of the nanoparticle absorption cross section will affect hot electron generation. For the [r_1, r_2] = [60, 76] nm nanoshells and [w, l] = [13, 47] nm nanorods used in these studies, the nanoshell to nanorod absorption cross section ratio is approximately four ($\sigma_{abs,NS} / \sigma_{abs,NR} \approx 4$), making it significantly more likely for hot electron-induced charge transfer to occur at the surface of a nanoshell.

Brus and coworkers have previously demonstrated that enhanced photochemistry can occur in areas of intense local fields at metal surfaces. [50,57,58] To evaluate the properties of plasmon-resonant local fields on nanoshells and nanorods specific to these studies, the near-field optical properties of nanoparticles of the dimensions used in our experiments were calculated using the Finite-Element Method (FEM), Figure 4. The dielectric function for Au determined by Johnson and Christy was used[59] and the nanoparticles were assumed to be embedded in H_2O (see methods for simulation details). For 800 nm laser excitation the maximum enhancements calculated for nanoshells ([r_1, r_2] = [60, 76] nm) and nanorods ([w, l] = [13, 47] nm) were 7 V/m, (Figure 4A, i) and 38 V/m (Figure 4A, ii), respectively. While the maximum electromagnetic field enhancement is largest for nanorod longitudinal excitation, this large local field is confined only to the tips of the rods and decays rapidly with increasing distance from the nanorod surface (Figure 4B, Nanorod). By comparison, the weaker local field on the nanoshell surface is distributed over a larger surface area and decays more slowly with increasing distance (Figure 4B, NS). Although the field enhancement maxima are larger on the nanorod surface, the surface area providing these large field enhancements is much smaller on the nanorod (Figure 4A, inset). If charge transfer correlates with regions of large local field on the nanoparticle surface, fewer DNA molecules would be susceptible to charge transfer-induced processes in a nanorod-based than in a nanoshell-based complex. For a single nanorod, assuming a uniform coverage of dsDNA on the nanorod surface, approximately 12 dsDNA strands (6 on each end) on average, would be located on the ends of the nanorod where the enhancements are the highest. Therefore, although a nonthermal mechanism for DNA release is in principle possible on any plasmonic nanoparticle surface, in the complexes fabricated for this series of experiments, the number of DNA molecules released by this mechanism, per nanoparticle, should be far greater from the nanoshell-based complex than from the nanorod-based complex.

If the transverse resonance is excited, then the local field will affect a greater number of dsDNA molecules, because the transverse plasmon would excite a greater area of the rod. However, the release of ssDNA upon transverse excitation with a 532 nm laser was not observed experimentally (Figure 3C). This result can most easily be explained because the transverse resonance is highly damped due to interband transitions, attenuating the near field for the transverse nanorod plasmon.

Additionally, in order to attach dsDNA to gold nanorods, an alkanethiol is required during the roundtrip phase transfer ligand exchange method. Although direct attachment of dsDNA to nanorods was attempted, it was determined that the roundtrip phase transfer ligand exchange method used for these set of experiments gave the most reliable and highest dsDNA surface coverage. The residual alkanethiol molecules on the surface of the nanorod could be playing a role in regards to the charge transfer process. This effect would only be noticed in areas of high electric field, where hot electrons are generated; and for nanorods, this area of enhanced electric field is much smaller compared to nanoshells. Further study may be needed to investigate the effect the alkanthiol has on light-triggered release.

Finally, the dsDNA packing density for these nanorod-dsDNA samples (~4.4 pmol/cm^2) presented in this article is approximately half that of nanoshells (~11.5 pmol/cm^2), which could potentially affect the light-triggered release process. However nanorod-dsDNA samples with packing densities comparable those on nanoshells (~120 DNA/nanorod, ~13.2 pmol/cm^2), still did not exhibit light-triggered release with the 800 nm laser excitation (supporting information, Figure S5). Additionally, the fluorescence intensity of the fluorescein-tagged DNA was unaffected by laser irradiation (supporting information, Figure S1).

Conclusion

We have examined the process of light-induced DNA release, relative to thermally induced DNA melting, on specially functionalized Au nanorod and nanoshell complexes. A clear distinction between light-induced DNA release, occurring at temperatures well below thermal release, and thermally-induced DNA release was observed on nanoshell-based complexes. For nanorod-based complexes treated under the same irradiation conditions only thermally-induced release of DNA was observed. In our experimental regime, where irradiation of the nanocomplexes is performed using low-intensity CW laser sources, the nanoparticle surface temperature increases appear minimal, and a nonequilibrium thermal mechanism involving high local temperatures at the nanoparticle surface appears unlikely for light-induced release. Instead, it appears quite feasible that the observed light-induced release may be explained by a nonthermal model, where hot electrons produced by plasmon decay are transferred to the adsorbate host-cargo system, facilitating dehybridization well below the DNA melting temperature. While both complexes should be responsive to such a release mechanism, differences in absorption cross sections and DNA densities on the nanoparticle surfaces render this effect observable only on nanoshell based complexes, for the present set of experimental conditions. Further examinations of this process should enable the development of light-induced release based vectors for a wide range of

nanoparticle morphologies, and the design of more efficient plasmonic nanoparticle-based delivery vectors.

Experimental Methods

Gold Nanoshell Fabrication

Au nanoshells were synthesized according to previously published procedures.[12,42] The dimensions of the silica core (120 nm colloidal silica, Precision Colloids LLC, Cartersville GA) and the Au shell were chosen such that the peak plasmon resonance in aqueous suspension was 800 nm, corresponding to the laser excitation wavelength used in this experiment.

Gold Nanorod Fabrication

Gold Nanorods were synthesized using a previous published CTAB seed-mediated growth method.[43] To make seed solution, 0.25 mL of 0.01M $HAuCl_4$ was mixed with 7.5 mL of 0.1M CTAB solution. Under vigorous stirring, 0.6 mL of ice-cold 0.01M $NaBH_4$ was quickly added. The solution turns from a golden yellow color to a pale brown color. It is essential that the temperature of $NaBH_4$ is maintained at ~0 °C prior to mixing with CTAB and $HAuCl_4$ for proper growth of nanorods. This solution was stored in a water bath at 27°C until further use. To make growth solution, 475 mL of 0.1M CTAB was combined with following solutions under slow stirring in the following order: 20 mL of 0.01M $HAuCl_4$, 3mL of 0.01M AgNO3, 3.20 mL of 0.1M Ascorbic acid. Addition of the Ascorbic acid changes the solution from yellow to colorless. Finally, 3.60 mL of the seed solution was added to the growth solution, then it was removed from the stirring plate and placed in a 27°C water bath for 2 hours. The reaction was both stopped and the nanorods were concentrated by centrifugation (6600 rcf, 20 min) and finally resuspended to 16 mL in Milli-Q water.

Ligand Exchange of Nanorods

The CTAB on the nanorod surface was replaced with mercaptohexanoic acid (MHA) using a previously reported roundtrip phase transfer ligand exchange method.[33,44] First the CTAB is replaced with dodecanethiol (DDT): 4 mL of the nanorod solution is placed in a glass vial and pure DDT is added on top. Upon the addition of acetone, the nanrods are extracted into the DDT organic phase by swirling for a few seconds. The aqueous phase becomes clear indicating ligand exchange. Next, the DDT organic phase is diluted with toluene and centrifuged to remove the excess DDT. Methanol may be needed to precipitate the nanorods prior to centrifugation. The supernatant was pipetted off and the DDT coated nanorods were resuspended in 2-3 mL of toluene by bath sonication for ~1 min. These DDT coated nanorods were then added to 9 mL of 0.01M MHA in toluene at ~80°C and vigorously stirred. Reflux and stirring continued until visible aggregation of the nanorods occurred (~10-12 min), which indicates that MHA has replaced the DDT, because MHA is insoluble in toluene. The solution was then allowed to cool to room temperature, washed twice with toluene and once with isopropanol via decantation. The isopropanol deprotonates the carboxylic acid. The aggregates resuspended in 1x Tris-Borate-EDTA (TBE) buffer.

DNA Functionalization of Nanoshells and Nanorods

DNA was hybridized by combining a thiolated sequence (5'- HS - $(CH_2)_6$ - TCAAGCTGTGACAGATCATA 3') with its complementary sequence that was tagged with a fluorophore on the 5' end (5'-FLUOROSCEIN-TATGATCTGTCACAGCTTGA-3') in a 1:1 M ratio. DNA hybridization was performed in DNA hybridization buffer (TE/50 mM NaCl, pH = 7.5). The solution was heated to 95°C then allowed to cool slowly to room temperature in a large water bath. The dsDNA was then precipitated with ethanol to minimize salt concentration and avoid nanoshell aggregation. For attaching dsDNA to nanoshells and to ensure the maximum surface dsDNA coverage on the nanoshells, excess hybridized dsDNA was incubated with an aqueous suspension of Au nanoshells for at least 8 h. The excess DNA was removed by centfifugation and the dsDNA-NSs were resuspended in 1x TE buffer (IDT, pH 7.5) For attaching dsDNA to nanorods charge screening is necessary to shield the negative charge of the phosphate backbone on the dsDNA with the negative charge on the ligand exchanged nanorods, which have mercaptohexanoic acid on them. This charge screening was performed using previously published methods.[33,44] The excess DNA was removed by centrifugation, and then the nanorords-dsDNA were resuspended in 1x TE buffer (IDT, pH = 7.5).

Thermal Treatment

A 3mL solution of the NS-dsDNA sample was placed in a centrifuge tube, then the centrifuge tube was placed in a water bath and the water bath was heated slowly (~1°C/ minute) while stirring. The slow heating and stirring ensures that the NS-dsDNA sample is in thermal equilibrium. The solution temperature is monitored by a thermocouple. The dehybridization and release of the fluorescein-tagged ssDNA is monitored by taking aliquots out of the solution as the solution temperature rises. Each aliquot is allowed to cool and then centrifuged, which separates the released DNA from the NSs. For each aliquot, the fluorescence intensity of the supernatant is measured, then by using a standard curve of fluorescence intensity versus DNA concentration, the concentration of DNA is quantified. Finally, dividing the DNA concentration by the nanoshell concentration, which is obtained from a UV-Vis extinction measurement, results in a quantitative DNA release curve.

Red Laser Treatment

Setup was the same as the thermal treatment, except the centrifuge tube was not placed in a water bath. The volume in all experiments was kept constant because the release of DNA was monitored as a function of solution temperature. Keeping the volume the same insures that any changes in the rate of heating are a result of the nanoparticle's photothermal properties and not the volume of solution. For the 800 nm laser a Diomed 15 Plus Laser was fibercoupled. The end of the fibercouple was placed above the sample (Power 1 W, Spot size Diameter = 1 cm, Optical Intensity = Power/Beam Cross section = 1.3 W/cm^2).

Green Laser Treatment

Setup was the same as the Red laser treatment. A Coherent Verdi 532 nm laser was used (Power = 1W, Spot size Diameter = 2.25 mm, Optical Intensity= 25 W/cm^2).

Near-field Calculations

Near-field optical properties were calculated using a commercially available Finite-Element Method (FEM) package (COMSOL Multiphysics 3.5). The total electric field was calculated in the frequency domain using the RF module. The particles are defined to have a Au dielectric function as determined by Johnson and Christy.[59] The particles were embedded in a surrounding spherical volume of water (eps=1.77). The surrounding medium is in turn embedded in a spherical perfectly matched layer (PML). The particles were excited with a plane wave. The simulation space is discretized into tetrahedral finite elements. The mesh size, simulation space volume, and PML thickness are chosen so that further changes in them do not affect the simulation results.

Instrumentation

Scanning electron microscope (SEM) images were obtained using a FEI Quanta 400 environmental SEM at an accelerating voltage of 25 k. Transmission electron microscope (TEM) images were taken using a using a JEOL JEM-2010 TEM. Extinction spectra were obtained using a Cary 5000 UV/vis/NIR spectrophotometer. Fluorescence emission were obtained using Jobin Yvon Fluoromax 3.

Total Extinction Cross Section

Total Extinction Cross Section = Particle concentration (Particles/mL) × Volume (cm^3) × theoretical extinction cross section/nanoparticle (cm^2). Theoretical Extinction cross section for nanoshell = 1.277×10^{-13} m^2 and for nanorods = $3.75\times10^{-14}m^2$.[48] For all experiments the total extinction cross section was normalized and checked experimentally by taking a UV-Vis of the solutions to confirm that both Nanoshell and nanorod solutions had the same extinction value.

Supplementary Material

Refer to Web version on PubMed Central for supplementary material.

Acknowledgments

This research was supported by the Robert A. Welch Foundation (C-1220 and C-1222), the Air Force Office of Scientific Research (FA9550-10-1-0469), the Office of Naval Research (N00014-10-1-0989), the National Science Foundation (IGERT) (DGE-0504425), the DoD NSSEFF (N00244-09-1-0067), the Center for Advanced Solar Photophysics, an Energy Frontier Research Center of the Department of Energy (78506-001-09), and the NIH (U01 CA 151886-01 and 5R01 CA151962-02). We thank Aoune Barhoumi, Surbhi Lal, and Britt Lassiter for helpful discussions.

References

1. Bardhan R, Chen WX, Bartels M, Perez-Torres C, Botero MF, McAninch RW, Contreras A, Schiff R, Pautler RG, Halas NJ, Joshi A. Nano Letters. 2010; 10:4920. [PubMed: 21090693]
2. Ghosh P, Han G, De M, Kim CK, Rotello VM. Advanced Drug Delivery Reviews. 2008; 60:1307. [PubMed: 18555555]
3. Thierry B. Current Drug Delivery. 2009; 6:391. [PubMed: 19534706]
4. Yamashita S, Fukushima H, Akiyama Y, Niidome Y, Mori T, Katayama Y, Niidome T. Bioorganic & Medicinal Chemistry. 2011; 19:2130. [PubMed: 21421321]
5. Sun YG, Mayers B, Xia YN. Advanced Materials. 2003; 15:641.

6. Chen J, Saeki F, Wiley BJ, Cang H, Cobb MJ, Li ZY, Au L, Zhang H, Kimmey MB, Li XD, Xia Y. Nano Letters. 2005; 5:473. [PubMed: 15755097]
7. Liang HP, Wan LJ, Bai CL, Jiang L. Journal of Physical Chemistry B. 2005; 109:7795.
8. Schwartzberg AM, Olson TY, Talley CE, Zhang JZ. Journal of Physical Chemistry B. 2006; 110:19935.
9. Skrabalak SE, Chen JY, Sun YG, Lu XM, Au L, Cobley CM, Xia YN. Accounts of Chemical Research. 2008; 41:1587. [PubMed: 18570442]
10. Jana NR, Gearheart L, Murphy CJ. Journal of Physical Chemistry B. 2001; 105:4065.
11. Norman TJ, Grant CD, Magana D, Zhang JZ, Liu J, Cao DL, Bridges F, Van Buuren A. Journal of Physical Chemistry B. 2002; 106:7005.
12. Brinson BE, Lassiter JB, Levin CS, Bardhan R, Mirin N, Halas NJ. Langmuir. 2008; 24:14166. [PubMed: 19360963]
13. Weissleder R. Nature Biotechnology. 2001; 19:316.
14. Melancon MP, Lu W, Yang Z, Zhang R, Cheng Z, Elliot AM, Stafford J, Olson T, Zhang JZ, Li C. Molecular Cancer Therapeutics. 2008; 7:1730. [PubMed: 18566244]
15. El-Sayed IH, Huang XH, El-Sayed MA. Nano Letters. 2005; 5:829. [PubMed: 15884879]
16. Wu GH, Milkhailovsky A, Khant HA, Fu C, Chiu W, Zasadzinski JA. Journal of the American Chemical Society. 2008; 130:8175. [PubMed: 18543914]
17. Chen CC, Lin YP, Wang CW, Tzeng HC, Wu CH, Chen YC, Chen CP, Chen LC, Wu YC. Journal of the American Chemical Society. 2006; 128:3709. [PubMed: 16536544]
18. Braun GB, Pallaoro A, Wu GH, Missirlis D, Zasadzinski JA, Tirrell M, Reich NO. Acs Nano. 2009; 3:2007. [PubMed: 19527019]
19. Loo C, Hirsch L, Lee MH, Chang E, West J, Halas NJ, Drezek R. Optics Letters. 2005; 30:1012. [PubMed: 15906987]
20. Anger P, Bharadwaj P, Novotny L. Physical Review Letters. 2006:96.
21. Kuhn S, Hakanson U, Rogobete L, Sandoghdar V. Physical Review Letters. 2006:97.
22. Tam F, Goodrich GP, Johnson BR, Halas NJ. Nano Letters. 2007; 7:496. [PubMed: 17256995]
23. Stranik O, Nooney R, McDonagh C, MacCraith BD. Plasmonics. 2007; 2:15.
24. Cade NI, Ritman-Meer T, Kwakwa KA, Richards D. Nanotechnology. 2009:20.
25. Sharrna P, Brown S, Walter G, Santra S, Moudgil B. Advances in Colloid and Interface Science. 2006; 123:471. [PubMed: 16890182]
26. Hahn MA, Singh AK, Sharma P, Brown SC, Moudgil BM. Analytical and Bioanalytical Chemistry. 2011; 399:3. [PubMed: 20924568]
27. Knight MW, Sobhani H, Nordlander P, Halas NJ. Science. 2011; 332:702. [PubMed: 21551059]
28. Link S, Ei-Sayed MA. Annual Review of Physical Chemistry. 2003; 54:331.
29. Jin RC, Cao YW, Mirkin CA, Kelly KL, Schatz GC, Zheng JG. Science. 2001; 294:1901. [PubMed: 11729310]
30. Redmond PL, Brus LE. Journal of Physical Chemistry C. 2007; 111:14849.
31. Lindstrom CD, Zhu XY. Chemical Reviews. 2006; 106:4281. [PubMed: 17031987]
32. Takahashi H, Niidome Y, Yamada S. Chemical Communications. 2005:2247. [PubMed: 15856111]
33. Wijaya A, Schaffer SB, Pallares IG, Hamad-Schifferli K. Acs Nano. 2009; 3:80. [PubMed: 19206252]
34. Pan Y, Neuss S, Leifert A, Fischler M, Wen F, Simon U, Schmid G, Brandau W, Jahnen-Dechent W. Small. 2007; 3:1941. [PubMed: 17963284]
35. Pan Y, Leifert A, Ruau D, Neuss S, Bornemann J, Schmid G, Brandau W, Simon U, Jahnen-Dechent W. Small. 2009; 5:2067. [PubMed: 19642089]
36. Poon L, Zandberg W, Hsiao D, Erno Z, Sen D, Gates BD, Branda NR. Acs Nano. 2010; 4:6395. [PubMed: 20958080]
37. Jones MR, Millstone JE, Giljohann DA, Seferos DS, Young KL, Mirkin CA. Chemphyschem. 2009; 10:1461. [PubMed: 19431161]
38. Lee SE, Liu GL, Kim F, Lee LP. Nano Letters. 2009; 9:562. [PubMed: 19128006]

39. Barhoumi A, Huschka R, Bardhan R, Knight MW, Halas NJ. Chemical Physics Letters. 2009; 482:171.
40. Zuloaga J, Prodan E, Nordlander P. Acs Nano. 2010; 4:5269. [PubMed: 20698558]
41. Prodan E, Radloff C, Halas NJ, Nordlander P. Science. 2003; 302:419. [PubMed: 14564001]
42. Oldenburg SJ, Averitt RD, Westcott SL, Halas NJ. Chemical Physics Letters. 1998; 288:243.
43. Sau TK, Murphy CJ. Langmuir. 2004; 20:6414. [PubMed: 15248731]
44. Wijaya A, Hamad-Schifferli K. Langmuir. 2008; 24:9966. [PubMed: 18717601]
45. Demers LM, Mirkin CA, Mucic RC, Reynolds RA, Letsinger RL, Elghanian R, Viswanadham G. Analytical Chemistry. 2000; 72:5535. [PubMed: 11101228]
46. Sun Y, Harris NC, Kiang CH. Physica a-Statistical Mechanics and Its Applications. 2005; 350:89.
47. Yamashita S, Fukushima H, Akiyama Y, Niidome Y, Mori T, Niidome T. Bioorganic and Medicinal Chemistry. 2011; 19:2130. [PubMed: 21421321]
48. Cole JR, Mirin NA, Knight MW, Goodrich GP, Halas NJ. Journal of Physical Chemistry C. 2009; 113:12090.
49. Maillard M, Huang PR, Brus L. Nano Letters. 2003; 3:1611.
50. Brus L. Accounts of Chemical Research. 2008; 41:1742. [PubMed: 18783255]
51. Wu XM, Thrall ES, Liu HT, Steigerwald M, Brus L. Journal of Physical Chemistry C. 2010; 114:12896.
52. Baffou G, Quidant R, de Abajo FJG. Acs Nano. 2010; 4:709. [PubMed: 20055439]
53. Baffou G, Quidant R, Girard C. Applied Physics Letters. 2009:94.
54. Govorov AO, Richardson HH. Nano Today. 2007; 2:30.
55. Govorov AO, Zhang W, Skeini T, Richardson H, Lee J, Kotov NA. Nanoscale Research Letters. 2006; 1:84.
56. Richardson HH, Carlson MT, Tandler PJ, Hernandez P, Govorov AO. Nano Letters. 2009; 9:1139. [PubMed: 19193041]
57. Nitzan A, Brus LE. Journal of Chemical Physics. 1981; 74:5321.
58. Nitzan A, Brus LE. Journal of Chemical Physics. 1981; 75:2205.
59. Johnson PB, Christy RW. Physical Review B. 1972; 6:4370.

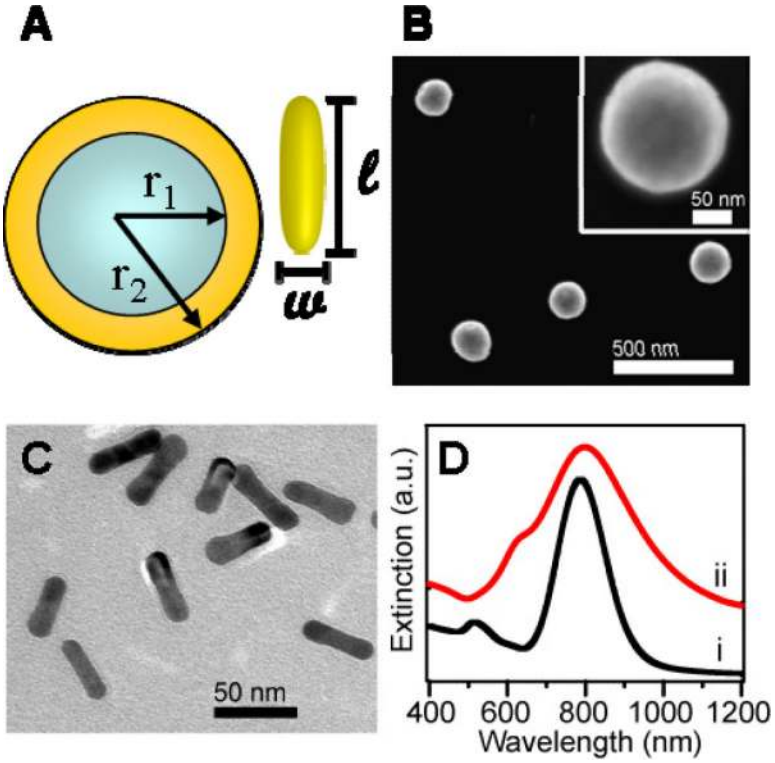

Figure 1.

(A) schematic of nanoshells ([r_1, r_2] = [60, 76] nm) and nanorods ([w, l] = [13, 47] nm) used in this series of experiments. (B) SEM image of nanoshells and (C) TEM image of nanorods. (D) Extinction spectra of solution of (i) nanorods with ($\lambda_{max} \approx 788$ nm) and (ii) nanoshells with ($\lambda_{max} \approx 797$ nm). Spectra are slightly vertically offset for clarity.

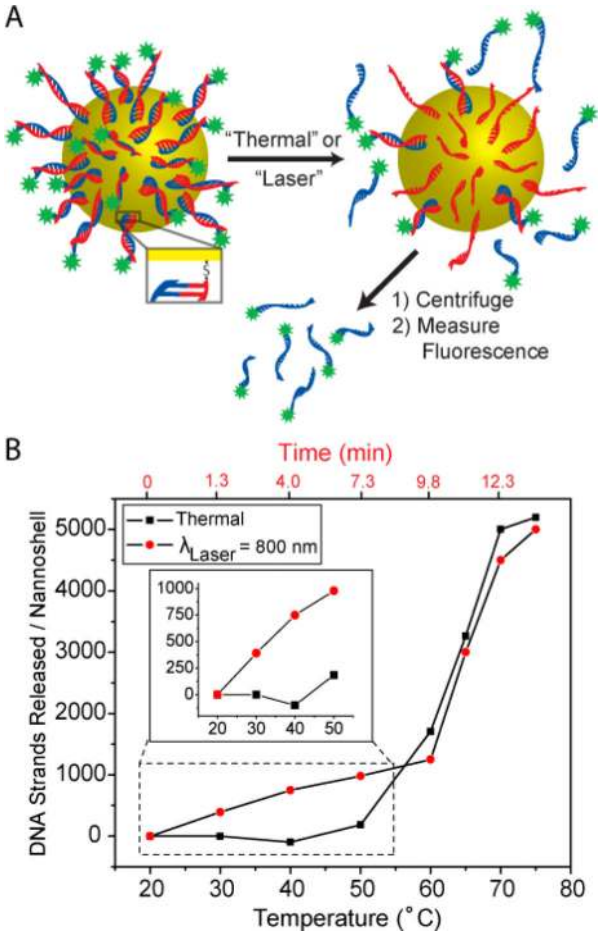

Figure 2.

Thermal and Light-Triggered release of ssDNA from nanoshells. (A) Schematic of ssDNA release from gold nanoshells. The thiolated host sequence (red) attaches to the gold surface. The cargo complementary sequence (blue) is tagged with a fluorescein molecule (green). Upon heating (thermal treatment) or illumination with laser light (laser treatment) the fluorescein-tagged sequence is released and subsequently separated from the nanoshells by centrifugation. The fluorescence is then measured and normalized by nanoshell concentration. (B) Number of DNA strands released per nanoshell as a function of solution temperature for thermal treatment (black squares) and laser treatment (red dots). The inset shows the expanded view of the temperature range prior to thermal melting where light-triggered release is observed.

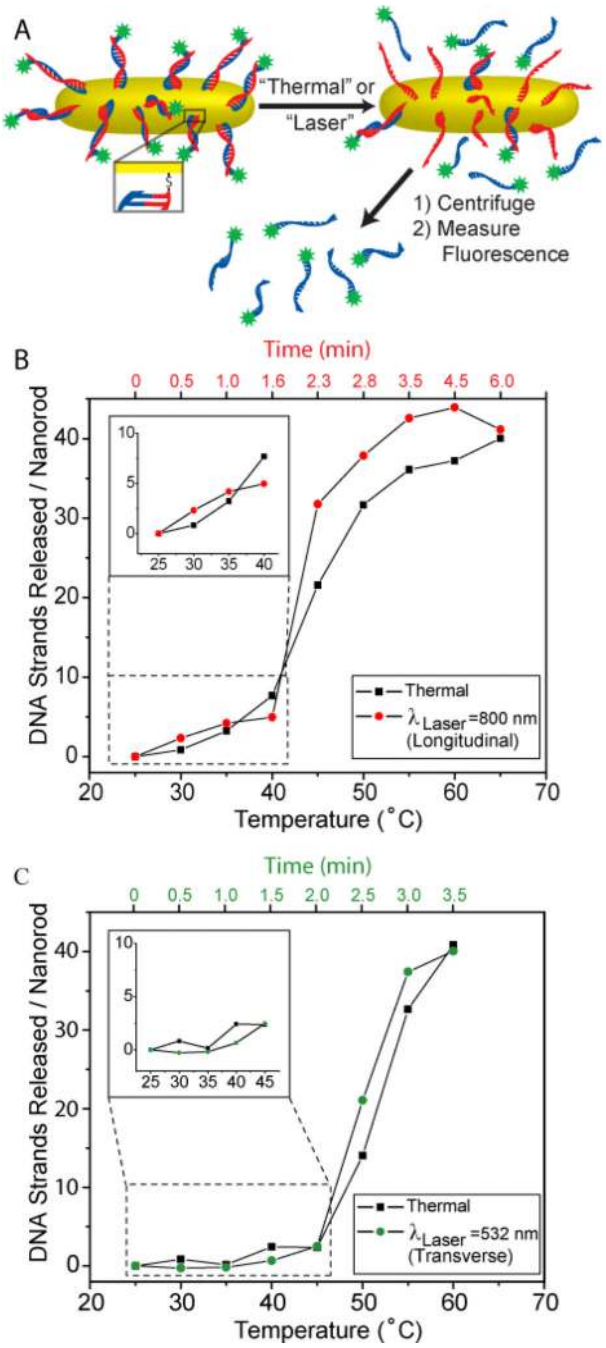

Figure 3.

Thermal and Light-Triggered Release of ssDNA from Au nanorods. (A) Schematic of ssDNA release. The thiolated sequence (red) attaches to the gold surface. The complementary sequence (blue) is tagged with a fluorescein molecule (green). Upon heating (thermal treatment) or illumination with laser light (laser treatment) the blue sequence is released and separated from the nanorods by centrifugation. The fluorescence is then measured and normalized by nanorod concentration. (B-C) Number of DNA strands released per nanorod as a function of solution temperature for thermal treatment (black

squares) and laser treatment with either (B) a near-infrared laser (λ_{laser}=800 nm) at the longitudinal resonance of the nanorod (red dots) or (C) a visible green laser (λ_{laser}=532 nm) at the transverse resonance of the nanorod (green dots). The inset shows the expanded view of the temperature range prior to thermal melting where light-triggered release is not observed.

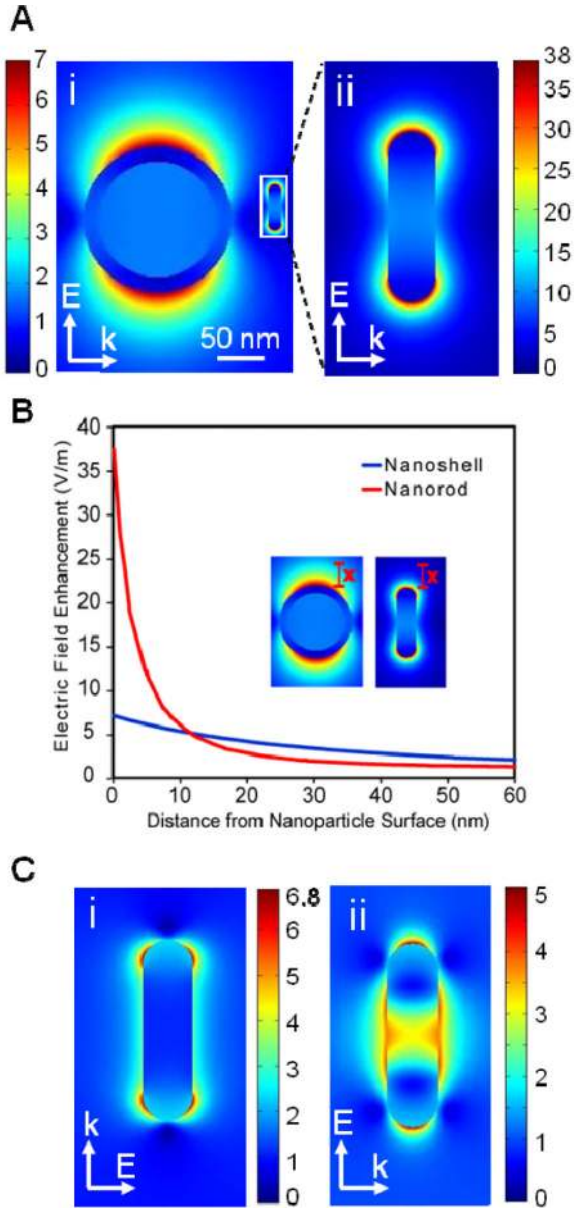

Figure 4.

Near-field intensity enhancements of nanoshells ([$r1$, $r2$] = [60, 76] nm) and nanorods ([w, l] = [13, 47] nm) calculated using the Finite-Element Method (FEM). (A) Enhancements for a (i) nanoshell and (ii) nanorod (longitudinal polarization) when driven at λ = 800 nm. Inset of nanorod depicts the size difference between nanoshells and nanorods. (B) Electric field enhancement as a function of distance from the nanoparticle surface in the polarization direction for nanoshells (blue) and nanorods (red). (C) Nanorod enhancements when driven at λ = 532 nm for: (i) transverse polarization and (ii) longitudinal polarization.